

Contribution of weak localization to non local transport at normal metal / superconductor double interfaces

R. Melin

Centre de Recherches sur les Très Basses Températures, CRTBT*,
CNRS, BP 166, 38042 Grenoble Cedex 9, France

In connection with a recent experiment [Russo et al., Phys. Rev. Lett. 95, 027002 (2005)], we investigate the effect of weak localization on non local transport in normal metal / insulator / superconductor / insulator / normal metal (NISIN) trilayers, with extended interfaces. The negative weak localization contribution to the crossed resistance can exceed in absolute value the positive elastic cotunneling contribution if the normal metal phase coherence length or the energy are large enough.

PACS numbers: 74.50.+r, 74.78.Na, 74.78.Fk

I. INTRODUCTION

The manipulation of correlated pairs of electrons in solid state devices has aroused a considerable interest recently. The goals of this line of research are the realization of sources of entangled pairs of electrons for quantum information, and the realization of fundamental tests of quantum mechanics^{1,2}. Correlated pairs of electrons can be extracted from a superconductor by Andreev reflection, with extended or localized interfaces between superconductors and normal metals or ferromagnets^{3,4,5,6,7,8,9}, and in Josephson junctions involving a double bridge between two superconductors¹⁰.

Charge is transported by Andreev reflection at a normal metal / superconductor (NS) interface: an electron coming from the normal side is reflected as a hole while a Cooper pair is transmitted in the superconductor¹¹. In the superconductor, Andreev reflection is mediated by an evanescent state of linear dimension set by the superconducting coherence length ξ . In structures in which a superconductor is multiply connected to normal metal electrodes separated by a distance of order ξ ^{12,13}, the Andreev reflected hole in the spin-() band can be transmitted in an electrode different from the one in which the incoming spin- electron propagates. This "non local" transmission in the electron-hole channel is called "crossed Andreev reflection". Non local transmission in the electron-electron channel corresponds to "elastic cotunneling" by which an electron is transmitted from one electrode to another while spin is conserved¹⁴.

A schematic three-terminal device is represented on Fig. 1, as well as the voltages V_a and V_b applied on the normal electrodes "a" and "b" respectively. The voltage V_s on the superconductor is chosen as the reference voltage ($V_s = 0$). Non local transport is characterized by a current $I_a(V_b)$ circulating in electrode "a" in response to a voltage V_b on electrode "b". It is supposed in addition that $V_a = 0$: electrode "a" is grounded, like in experiments^{8,9} (see Fig. 1). The crossed conductance is defined by $G_{a,b}(V_b) = \partial I_a / \partial V_b(V_b)$. A crossed conductance dominated by elastic cotunneling (crossed Andreev reflection) is negative (positive)¹⁵ because of the

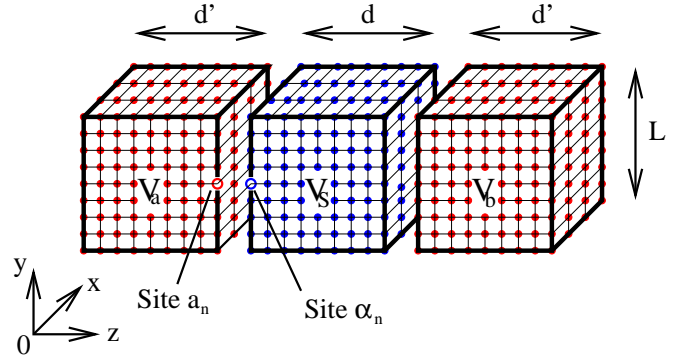


FIG. 1: (Color online.) Schematic representation of the tight-binding model of NISIN trilayer. The insulating layers are not shown on the figure. The aspect ratio is not to the scale of the experiment in Ref. 9 for which $d = 15; 50; 200$ nm, L is of order of $5 \mu\text{m}$, and $d' \sim 50$ nm.

opposite charges of the outgoing particle in elastic cotunneling and crossed Andreev reflection. Lowest order perturbation theory in the tunnel amplitudes leads to $G_{a,b}(V_b) = 0$ because the crossed Andreev reflection and elastic cotunneling channels have in this case an exactly opposite contribution to the crossed conductance once the average over disorder^{16,17} or over the Fermi oscillations in multichannel ballistic systems^{14,18} is taken into account.

Three unexpected experimental features for the crossed conductance in a normal metal / insulator / superconductor / insulator / normal metal (NISIN) trilayer have been reported recently by Russo et al.⁹: i) The crossed conductance does not average to zero with normal metals, in contradiction to the aforementioned prediction of lowest order perturbation theory in the tunnel amplitudes¹⁴. The order of magnitude of the experimentally observed crossed signal is far from being compatible with lowest order perturbation theory. ii) A magnetic field applied parallel to the interfaces suppresses the non local signal, suggesting a phase coherent process. iii) The sign of the crossed resistance¹⁵ crosses over from positive (the sign of elastic cotunneling) to negative (the

sign of crossed Andreev reflection) as the bias voltage V_b increases, and the crossed signal disappears if the bias voltage exceeds the Thouless energy in the superconductor.

We show here that weak localization with extended interfaces leads to a positive crossed conductance, the sign of which is opposite to the sign of the dominant elastic cotunneling channel for localized interfaces¹⁹. The weak localization contribution to the crossed conductance becomes important at large bias voltages and for a large phase coherence length in the normal metals.

The article is organized as follows. Necessary preliminaries are given in Sec. II. The weak localization contribution to crossed transport is discussed in Sec. III. Concluding remarks are given in Sec. IV.

II. PRELIMINARIES

A. Hamiltonians

The normal metal electrodes are described by the tight binding Hamiltonian

$$H_N = \sum_{\mathbf{k}} (\mathbf{k}) c_{\mathbf{k}}^\dagger c_{\mathbf{k}}; \quad (1)$$

where \mathbf{k} is the wave-vector, $\sigma = \uparrow, \downarrow$ the projection of the electron spin on the spin quantization axis, and where $(\mathbf{k}) = 2t_0 [\cos(k_x a_0) + \cos(k_y a_0) + \cos(k_z a_0)]$ is the dispersion relation of free electrons on a cubic lattice, with t_0 the bulk hopping amplitude, a_0 the distance between two neighboring sites, and k_x, k_y and k_z the projections of the electron wave-vector on the x, y and z axis (see Fig. 1).

The superconductor is described by the BCS Hamiltonian

$$H_{BCS} = \sum_{\mathbf{k}} (\mathbf{k}) c_{\mathbf{k}}^\dagger c_{\mathbf{k}} + \sum_{\mathbf{k}} c_{\mathbf{k}, \uparrow}^\dagger c_{\mathbf{k}, \downarrow}^\dagger + c_{\mathbf{k}, \downarrow} c_{\mathbf{k}, \uparrow}; \quad (2)$$

with the superconducting gap.

Diagonal disorder is included²⁰, with an elastic mean free path $l_e^{(N)}$ in the normal electrodes of the NISIN trilayer, and $l_e^{(S)}$ in the superconducting electrode. A finite coherence length $l^{(N)}$ in the normal electrodes is accounted for by adding phenomenologically an imaginary part to the energy.

At the extended interface $a-$, the tunnel Hamiltonian connecting the electrodes a and s takes the form

$$\hat{W}_{a-} = \sum_{n_i} t c_{a_n}^\dagger c_{n_i} + c_{n_i}^\dagger c_{a_n}; \quad (3)$$

where the sites a_n on the normal metal side of the interface correspond to the sites n_i on the superconducting side of the interface (see Fig. 1), and a similar expression holds for the tunnel Hamiltonian at the interface $b-$.

B. Green's functions

The fully dressed advanced and retarded equilibrium Nambu Green's function $\hat{G}^{A,R}(\omega)$ at energy ω is first determined by solving the Dyson equation

$$\hat{G}^{A,R}(\omega) = \hat{g}^{A,R}(\omega) + \hat{g}^{A,R}(\omega) \hat{\Sigma}_t \hat{G}^{A,R}(\omega); \quad (4)$$

where \sum_t denotes a summation over the spatial indices, and $\hat{g}^{A,R}(\omega)$ are the advanced and retarded Green's functions of the disconnected system (i. e. with $t=0$ in the tunnel Hamiltonian given by Eq. (3)). The self-energy $\hat{\Sigma}_t$ corresponds to the couplings in the tunnel Hamiltonian given by Eq. (3). The Green's functions are 4×4 matrices in the spin Nambu representation. The four components correspond to a spin-up electron, a spin-down hole, a spin-down electron and a spin-up hole. Because of spin rotation invariance, some elements of the 4×4 Green's functions are redundant. We work here in a 2×2 block in the sector $S_z = \pm 1/2$, encoding the superconducting correlations among a spin-up electron (Nambu label $\backslash 1$) and a spin-down hole (Nambu label $\backslash 2$).

Once the fully dressed advanced and retarded Green's functions have been obtained, the Keldysh Green's function \hat{G}^{+} is determined by the Dyson-Keldysh equation^{21,22,23,24,25}

$$\hat{G}^{+} = \hat{I} + \hat{G}^R \hat{\Sigma}_t \hat{g}^{+} \hat{I} + \hat{\Sigma}_t \hat{G}^A; \quad (5)$$

where \hat{g}^{+} is the Keldysh Green's function of the isolated electrodes, and where the energy dependence of the Green's functions is omitted.

C. Transport formula

The current through the interface $a-$ is given by

$$I_{a-} = \frac{2e}{h} \sum_{\mathbf{n}} \text{Tr} \left[\hat{t}_{a_n} \hat{G}_{n_i a_n}^{+}(\omega) \right] \quad (6)$$

where the trace is a summation over the two components of the Nambu Green's function, $\hat{\sigma}_3$ is one of the Pauli matrices, the diagonal elements of which are $(1; -1)$, and the sum over n runs over all sites at the interface $a-$. As shown on Fig. 1, the symbols a_n and n_i in Eq. (6) label two corresponding sites at the interface, in the normal electrode a and in the superconductor respectively. The two spin orientations are taken into account in the prefactor of Eq. (6).

The local conductance of a NIN interface is equal to $(e^2/h)T$ per channel, where $T = 2^{-2} t^2 \rho_N$ is the dimensionless transmission coefficient in the tunnel limit, with ρ_N the normal density of states²¹.

The non perturbative transport formula for the local current at a localized NIN interface was obtained in

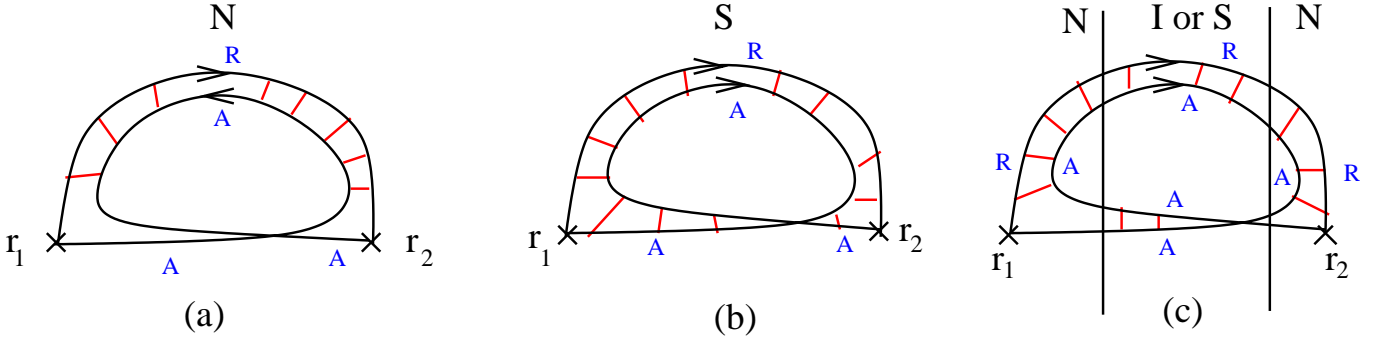


FIG. 2: (Color online.) A weak localization diagram in a normal metal for which r_1 and r_2 are within the elastic mean free path l_e (a), and in a superconductor for which r_1 and r_2 are within ξ (b). (c) represents the same diagram at a NISIN double interface, equivalent to Fig. 3c. In the NISIN case on (c) r_1 and r_2 are within ξ and r_1, r_2 are within $l_e^{(N)}$ from the interfaces. In the NIN case on (c), r_1 and r_2 are within the insulator correlation length. "A" and "R" stand for advanced and retarded.

Ref. 21, and generalized in Ref. 25 to a localized NIS interface, and in Ref. 19 to non local transport at a double ferromagnet / superconductor interface. We deduce from these references the exact expressions of the local conductance $G_{NIN}(V)$ of a single NIN interface, of the Andreev conductance $G_{NIS}(V)$ of a single NIS interface, and of the crossed conductance $G_{a,b}(V_b)$ of a NISIN trilayer with extended interfaces:

$$G_{NIN}(V) = \frac{8}{h} \frac{e^2}{h} t^4 \sum_{j,k;l} \overline{G_{a_1;a_j}^A(i;l;k)(eV)} \overline{G_{b_k;b_1}^R(i;l;k)(eV)} \quad (7)$$

$$G_{NIS}(V) = \frac{16}{h} \frac{e^2}{h} t^4 \sum_{j,k;l} \overline{G_{a_1;a_j}^A(i;l;k)(eV)} \overline{G_{b_k;b_1}^R(i;l;k)(eV)} \quad (8)$$

$$G_{a,b}(V_b) = \frac{8}{h} \frac{e^2}{h} t^4 \sum_{j,k;l} \overline{\text{Tr} \left(\hat{G}_{a_1;a_j}^A(i;l;k)(eV_b) \hat{G}_{b_k;b_1}^R(i;l;k)(eV_b) \right)} \quad (9)$$

valid to all orders in the hopping amplitude. The crossed conductance $G_{a,b}(V_b)$ is per conduction channel through the junction of area $L \times L$, with a superconducting layer of thickness d (see Fig. 1). The summations in Eqs. (8) and (9) run over all pairs of sites at the interfaces, and the overline denotes disorder averaging. The density of states $\hat{G}_{a_1;a_j}^A = (\hat{G}_{a_1;a_j}^A - \hat{G}_{a_1;a_j}^R)/2i$ connects the sites a_1 and a_j in electrode "a", and a similar definition holds for $\hat{G}_{b_k;b_1}^R$. The site a_j (b_1) in electrode "a" ("b") is connected by the tunnel Hamiltonian to the site j (1) in the superconductor (see Fig. 3 for the NISIN interface). In the case of the local conductance of a NIN junction, $j, k, 1$ and i belong to an insulating layer that has been inserted in between the two normal metals. The tunnel amplitude t in Eq. (7) connects in this case the normal metal to the insulator, while t in Eqs. (8) and (9) connects the normal metal to the superconductor.

The fully dressed advanced and retarded equilibrium Nambu Green's functions $\hat{G}_{j;k}^A(i;l;k)(eV)$ and $\hat{G}_{1;i}^R(i;l;k)(eV)$ at energy i in Eqs. (7), (8) and (9) are expanded by using the Dyson equation given by Eq. (5). We deduce from the exact Keldysh transport formula given by Eqs. (7), (8) and (9) that the diagrams are connected, and that the propagators for the density of states are directly connected to at least one tunneling vertex. The other extremity of the density of states propagators is connected either to a tunneling vertex, or to a disorder scattering vertex. The density of states, represented by wavy lines on the diagrams, connects to one advanced and one retarded Green's function as in Eqs. (7), (8) and (9).

A crossed conductance dominated by elastic cotunneling (crossed Andreev reflection) is negative (positive)¹⁵. This can be seen most simply by making the Nambu labels explicit in Eq. (9) and taking into account the signs in the γ_3 matrices, and the global sign.

The crossed conductance is expanded perturbatively in T^2 , where the normal local transmission coefficient T has already been defined, and is also expanded in the number of non local processes crossing the superconductor since $d \ll \xi$ ¹⁴.

D. Weak localization in a superconductor

Weak localization in a superconductor was already investigated in Ref. 26 in connection with the determination of the number density of superconducting electrons. A weak localization diagram in a bulk normal metal is shown on Fig. 2a. In this case the two points r_1 and r_2 are within the elastic mean free path $l_e^{(N)}$. In a bulk superconductor (see Fig. 2b), the two points r_1 and r_2 are within the coherence length ξ since the disorder average $\overline{g^A}; \overline{g^R}$ of two advanced Green's functions between the two sites and at r_1 and r_2 in a superconductor is limited by ξ , not by l_e . Similar diagrams for the conductance are introduced at a NISIN double interface in Sec. III. In this case the points r_1 and r_2 are separated

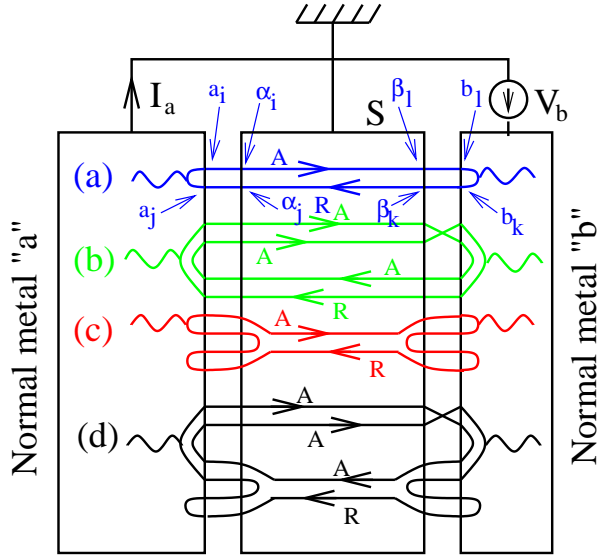


FIG. 3: (Color online.) The lowest order diagrams contributing to crossed transport. We show (a) the vanishing diagram of order T^2 , (b) the vanishing weak localization diagram of order T^4 , (c) the first non vanishing diagram of order T^4 , and (d) the weak localization diagram of order T^6 . The wavy lines correspond to the insertion of the normal metal density of states, and of a \hat{G}_3 matrix.

by the superconductor thickness, of order λ (see Fig. 2c). At a N|N interface, the two points r_1 and r_2 on different interfaces can be separated by a distance equal to the thickness of the insulator, comparable to the decay length induced by the charge gap of the insulator.

III. NON LOCAL TRANSPORT IN A N|S|N TRILAYER

A. Crossed conductance to order T^2

Now we evaluate the lowest order diagrams appearing in the crossed conductance of a N|S|N trilayer. The crossed conductance due to the diagram of order T^2 (see Fig. 3a) vanishes because the contributions of the elastic cotunneling and crossed Andreev reflection channels are exactly opposite^{14,16,18,19}. This can be seen also by evaluating the summation over the Nambu labels in the diagram on Fig. 3 and using $\bar{g}_{i;1}^{1;1} \bar{g}_{i;1}^{1;1} = \bar{g}_{i;2}^{1;2} \bar{g}_{i;2}^{2;1}$, where i and j are two points in the superconductor at a distance of order λ .

B. Crossed conductance to order T^4

The first weak localization diagram of order T^4 involving four Green's functions in the superconductor is shown on Fig. 3b. The corresponding crossed conductance vanishes, as for the diagram of order T^2 discussed

in Sec. III A.

The diagram of order T^4 on Fig. 3c takes a finite value, and is evaluated explicitly by summing over all possible Nambu labels, and over the different possibilities of inserting the density of states and the \hat{G}_3 matrices (represented by the wavy lines on the diagrams). This leads to the crossed conductance

$$G_{a,b}(V_b) = 4 \frac{2t^8}{N} \sum \frac{\bar{g}_{i;1}^{1;1;A}(eV_b) \bar{g}_{i;2}^{2;2;R}(eV_b)}{\bar{g}_{i;1}^{1;2;A}(eV_b) \bar{g}_{i;2}^{1;2;R}(eV_b)} \frac{2}{(eV_b)^2}; \quad (10)$$

where¹⁹

$$\begin{aligned} \bar{g}_{i;1}^{1;1}(\epsilon) \bar{g}_{i;2}^{2;2}(\epsilon) &= \frac{2}{2} \frac{S}{S} (R) \exp \left[-\frac{2R}{(\epsilon)} \frac{2!^2}{2!^2} \right] \\ \bar{g}_{i;1}^{1;2}(\epsilon) \bar{g}_{i;2}^{1;2}(\epsilon) &= \frac{2}{2} \frac{S}{S} (R) \exp \left[-\frac{2R}{(\epsilon)} \frac{2}{2!^2} \right]; \end{aligned}$$

with R the distance between the sites i and j , and with $(R) = (k_F R)^2$ in the ballistic limit, and $(R) = k_F^2 R \lambda_e^{(S)}$ in the diffusive limit. The resulting term of order T^4 in the crossed conductance is given by

$$G_{a,b}^{(ec)}(V_b) = \frac{e^2}{h} T^4 \frac{2}{\lambda_e^{(S)}} \frac{2}{(eV_b)^2} \exp \left[-\frac{2d}{\lambda_e^{(S)}} \right]; \quad (11)$$

in agreement with the expansion to order T^4 of the crossed conductance obtained for highly transparent localized interfaces¹⁹. A summation over the pairs of sites i and j at the two interfaces was carried out, giving rise to the prefactor $= \frac{1}{\lambda_e^{(S)}}$ in Eq. (11).

C. Weak localization diagram of order T^6

1. Contribution of local excursions

We consider now the weak localization diagram of order T^6 on Fig. 3d, merging the features of the two diagrams of order T^4 on Figs. 3b and c, and shown in more details on Fig. 4. The long range propagation in the normal electrodes involves the diffusons $\bar{g}_{i;1}^{A;1;1;R} \bar{g}_{i;2}^{R;1;1;A}$ and $\bar{g}_{i;1}^{A;2;2;R} \bar{g}_{i;2}^{R;2;2;A}$ in the particle-particle or hole-hole channel (where i and j belong to the normal electrode), as opposed to the diffuson $\bar{g}_{i;1}^{A;1;1;A} \bar{g}_{i;2}^{A;2;2;A}$ in the particle-hole channel for local Andreev reflection at a single N|S interface^{27,28} below the related Thouless energy.

We first evaluate the part of the diagram on Fig. 4 involving local excursions at the N|S interfaces (see Fig. 5). Enumerating these diagrams shows that the two local excursions are attached to the same non local propagation in the superconductor. We use the notation $X_{i;0;0}^{A;A;0;0}$ ($X_{i;0;0}^{A;R;0;0}$) for the part of the diagram on Fig. 5 with two advanced (one advanced and one retarded) propagators

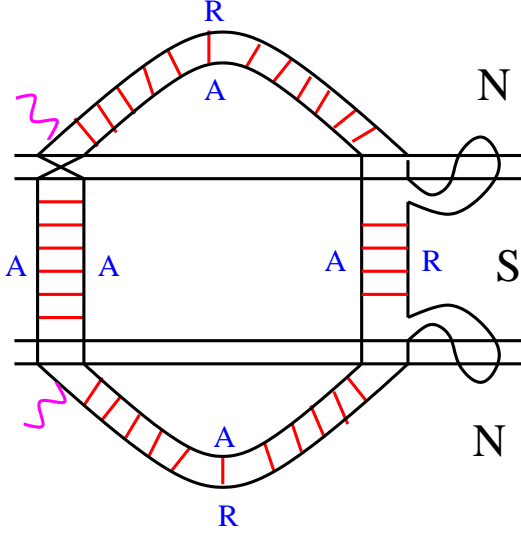


FIG. 4: (Color online.) Details of the insertion of the densities of states and of the $\hat{\gamma}_3$ matrices in the weak localization diagram on Fig. 3d. "A" and "R" stand for advanced and retarded. The diagrams are calculated in the ladder approximation. The rungs of the ladders represented by the red lines represent schematically the diagram in the ladder approximation.

in the superconductor, and the Nambu labels $(\uparrow; \uparrow)$ and $(\uparrow; \downarrow)$ at the extremities in the two normal electrodes. We find

$$X_{11;11}^{A;A} = X_{11;22}^{A;A} = \frac{8}{(R)} \frac{2}{(2)} \frac{6}{(2)} \frac{1}{(2)} \frac{2}{(2)} \quad (12)$$

$$X_{11;11}^{A;R} = X_{11;22}^{A;R} = \frac{2}{(R)} \frac{2}{(2)} \frac{6}{(2)} \frac{2}{(2)} \quad (13)$$

We recover Eq. (11) for the non vanishing diagram of order T^4 on Fig. 3c, proportional to $(X_{11;11}^{A;R} - X_{11;22}^{A;R})$. The global minus sign in this expression can be found in Eq. (9), and the opposite signs for $X_{11;11}^{A;R}$ and $X_{11;22}^{A;R}$ are due to the matrices $\hat{\gamma}_3$ in Eq. (9). The diagram with local excursions attached to the disorder average of two advanced or two retarded Green's functions in the superconductor lead to a vanishingly small crossed conductance, as it can be seen from the identity $(X_{11;11}^{A;A} - X_{11;22}^{A;A}) = 0$, deduced from Eq. (12).

D. Weak localization crossed conductance

The weak localization contribution to the crossed conductance corresponding to the diagram on Fig. 4 is given by

$$G_{a,b}^{(w)}(eV_b) = G_{a,b}^{(ec)}(V_b) F \left(\frac{d}{L_F}; \frac{V_b}{L_F}; \frac{1}{L_F^{(N)}} \right) \quad (14)$$

where $G_{a,b}^{(ec)}(V_b)$ is given by Eq. (11) and

$$F \left(\frac{d}{L_F}; \frac{V_b}{L_F}; \frac{1}{L_F^{(N)}} \right) = \frac{1}{4} T^2 \frac{1}{L_F^{(N)}} \frac{1}{L_F^{(S)}} \frac{2}{(eV_b)^2} \exp \left(\frac{2d}{L_F} \right) \quad (15)$$

The sign of $G_{a,b}^{(w)}(eV_b)$ given by Eq. (14) is positive, as for crossed Andreev reflection. The factor $(L_F^{(N)} = L_F^{(S)})^4$ is due to a factor $(L_F^{(N)} = L_F^{(S)})^2$ associated to the diagrams in each of the quasi-two-dimensional normal layers [see Eq. (A5)] in the limit $q = 0$. The constraint $q = 0$ originates from the conservation of the component of the wave-vector parallel to the interface, due to the symmetry by translation parallel to the interfaces (see Appendix B).

It can be shown that the two diagrams of order T^6 involving a single diagram in the superconductor and long range propagation in the normal metals are negligible because of the sum over the Nambu labels in one diagram, and because of the factor $(L_F^{(N)} = L_F^{(S)})^2$ in the other diagram, much smaller than $(L_F^{(N)} = L_F^{(S)})^4$ for the weak localization diagram.

The weak localization crossed conductance can be expanded systematically in powers of $(L_F = L_F^{(N)})^2$:

$$G_{a,b}(eV_b = 0) = \frac{e^2}{h} \sum_n A_n(T) \frac{1}{L_F^{(N)}}^{2n} \quad (16)$$

The coefficients $A_n(T)$ are evaluated to leading order in T because of the small interface transparencies. Estimating the higher order weak localization diagrams leads to $A_3 \sim T^8$, $A_4 = 0$, $A_5 \sim T^{10}$, $A_6 = 0$, $A_7 \sim T^{12}$, ... The order of magnitude of the sum of the higher order contributions can be obtained from summing the corresponding geometric series for $T (L_F = L_F^{(N)})^2 > 1$: $\sum_{n=3}^{\infty} A_n(T) (L_F = L_F^{(N)})^{2n}$ is of order $T^2 (L_F = L_F^{(N)})^4$, much smaller than $A_2(T) (L_F = L_F^{(N)})^4$, therefore justifying why we based our discussion on the first two terms $A_0(T) T^4$ and $A_2(T) T^6$.

E. Relation to experiments

1. Determination of the parameters

The number of channels N_{ch} for a contact with a three-dimensional metal is $N_{ch} = S = \frac{2}{F}$, where S is the junction area and F the Fermi wave-length. The normal layers have a dimension $L \times L \times d^0$, with $L \sim 5 \mu m$ and a thickness $d^0 \sim 50 nm$ (see Fig. 1). The number of channels in the quasi-two-dimensional geometry is obtained by neglecting disorder (the elastic mean free path in the experiment is limited by scattering on the normal im-

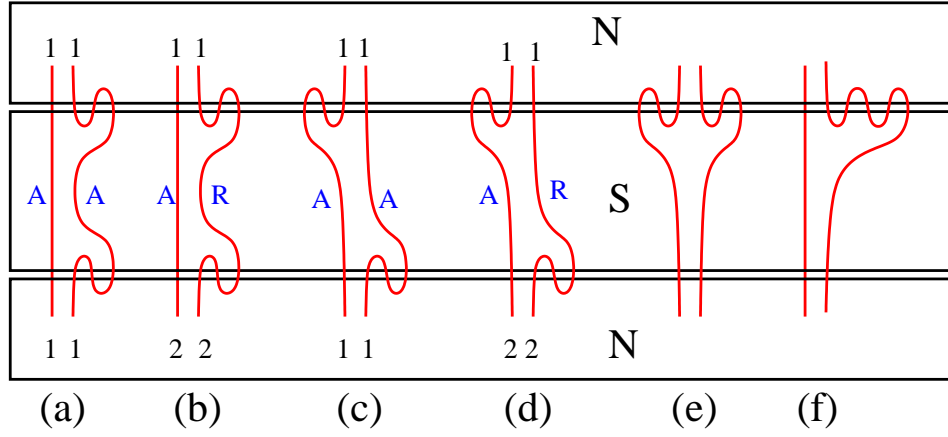


FIG. 5: (Color online.) Representation of the part of the diagram of order T^6 (see Fig. 3) with local excursions. $\backslash 1''$ and $\backslash 2''$ correspond to the Nambu labels. (a), (b), (c) and (d) contribute respectively to $X_{11;11}^{A,A}$, $X_{11;22}^{A,R}$, $X_{11;11}^{A,A}$ and $X_{11;22}^{A,R}$. The diagrams having the topology of (e) and (f) lead to a vanishingly small crossed conductance because of the matrices $\hat{\gamma}_3$ and the trace over the Nambu labels.

boundaries), and by evaluating the area of the Fermi surface with discrete wave-vectors in the direction perpendicular to the interface, leading to $N_{ch} = Ld^0 = \frac{2}{F}$, $6 \cdot 10^5$. The normal transparency T can be obtained from the local conductance in the normal state $R_N^{(loc)}$, 2 :

$$\frac{1}{R_N^{(loc)}} \sim 2N_{ch}T \frac{e^2}{h}; \quad (17)$$

leading to $T \sim 10^{-2}$. These values $T \sim 10^{-2}$ and $N_{ch} \sim 6 \cdot 10^5$ are compatible with the local Andreev resistance at zero bias of about 100 Ω , being an upper bound to the zero temperature Andreev resistance $R_A^{(loc)}$ given by $1/R_A^{(loc)} = 2(e^2/h)T^2N_{ch}$. Russo et al.⁹ estimate $T \sim 10^{-5}$ from $N_{ch} = S = \frac{2}{F}$ for a three dimensional metal. The possible dependence of N_{ch} on d^0 that we consider here can be probed experimentally by determining how the crossed resistance depends on the thickness of the normal layers.

2. Crossed resistance

The crossed resistance matrix measured experimentally⁹ is the inverse of the crossed conductance matrix. The off-diagonal element of the crossed resistance matrix is given by

$$R_{a,b}^{(tot)}(V_b) = \frac{G_{a,b}^{(tot)}(V_b)}{G_{a,a}^{(tot)}(V_b)G_{b,b}^{(tot)}(V_b) - G_{a,b}^{(tot)}(V_b)G_{b,a}^{(tot)}(V_b)}; \quad (18)$$

where $G_{a,a}^{(tot)}(V_b) = G_{b,b}^{(tot)}(V_b) = G_{loc}^{(tot)}(V_b)$ is the local Andreev conductance.

The elastic cotunneling crossed resistance correspond-

ing solely to the contribution of Eq. (11) is thus of order

$$R_{a,b}^{(ec)}(V_b = 0) = \frac{1}{4N_{ch}} \frac{h}{e^2} \frac{1}{l_e^{(S)}} \frac{2}{\exp(-2d^0)} \exp(-2d^0); \quad (19)$$

having an order of magnitude compatible with the experiment⁹. The elastic cotunneling crossed resistance is independent on T for tunnel interfaces. The elastic cotunneling crossed resistance $R_{a,b}^{(ec)}(V_b = 0)$ being inversely proportional to N_{ch} , with N_{ch} proportional to d^0 (see Sec. III E 1), it is expected that the crossed resistance would decrease if the normal metal layer thickness d^0 increases, as anticipated in Sec. III E 1.

Now, the weak localization crossed resistance is equal to

$$R_{a,b}^{(wl)} = R_{a,b}^{(ec)} F \left[-\frac{d}{l_e^{(N)}}; \frac{l_e^{(N)}}{l_e^{(N)}} \right]; \quad (20)$$

The voltage dependence of the total crossed resistance $R_{a,b}(V_b) = R_{a,b}^{(ec)}(V_b) + R_{a,b}^{(wl)}(V_b)$ is shown on Fig. 6 for different values of $l_e^{(N)} = l_e^{(N)}$. We obtain a change of sign from a positive (elastic cotunneling dominated) to a negative (weak localization dominated) crossed resistance as the voltage increases (see Fig. 6). For sufficiently large values of the phase coherence length, we have $F(d; 0; l_e^{(N)} = l_e^{(N)}) > 1$ as discussed above, so that the crossed resistance is negative for all values of the bias voltage.

The perturbative crossed resistance on Fig. 6 tends to a finite value in the limit $eV_b = 0$. The determination of the crossed conductance around $eV_b = 0$ is examined in Ref. 19 for localized interfaces with arbitrary interface transparencies. The non perturbative crossed conductance tends to zero for $eV_b = 0$, but the cross-over

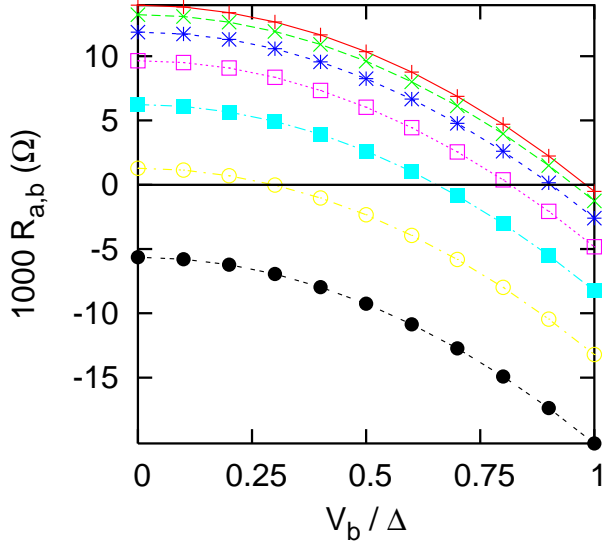


FIG. 6: (Color online.) Voltage dependence of the crossed resistance (in Ohms), given by Eq. (18), in which the crossed conductance is the sum of the elastic cotunneling [see Eq. (11)] and weak localization [see Eq. (14)] contributions. We used the parameters $d = 20 \text{ nm}$, $\ell = 15 \text{ nm}$, $l_e^{(N)} = 50 \text{ nm}$, $l_e^{(S)} = 3 \text{ nm}$, $T = 10^{-2}$, $N_{\text{ch}} = 6 \cdot 10^5$. The values of $l^{(N)}$ are, from top to bottom: $l^{(N)} = 0.4; 0.5; 0.6; 0.7; 0.8; 0.9; 1 \text{ μm}$. The points are theoretical, and the lines are a guide to the eye.

occurs within an energy window that becomes very small for tunnel interfaces. A crossed current related to out-of-equilibrium quasiparticle populations (not described here) is expected for $eV_b > \Delta$.

As it is visible on Fig. 6, the characteristic voltage scale in the bias voltage dependence of the crossed resistance is the superconducting gap, not the normal state superconductor Thouless energy obtained in experiments. At the present stage, we do not find a plausible explanation of this experimental observation.

F. Magnetic field dependence

The experimental crossed signal is suppressed by a magnetic field parallel to the layers⁹. The theoretical weak localization crossed signal is also suppressed by a magnetic field because the corresponding diagram dephases in an applied magnetic field. The cross-over magnetic field B_{c} for the suppression of the weak localization crossed conductance corresponds to one superconducting flux quantum Φ_0 enclosed in the area of the diagram, compatible with experiments⁹. However, in experiments, the crossed resistance is suppressed by a magnetic field in the entire voltage range. The present model does not explain the dephasing of the elastic cotunneling contribution.

IV. CONCLUSIONS

We have calculated the weak localization contribution to non local transport in NISIN trilayers with extended interfaces and a sufficient phase coherence length in the normal electrodes. We find a change of sign in the crossed resistance between elastic cotunneling at low voltages and weak localization at higher voltages. The weak localization contribution can dominate for all voltages if the phase coherence length is large enough. The weak localization crossed conductance dephases in an applied magnetic field, but not the elastic cotunneling contribution. The appearance of a voltage scale related to the superconductor Thouless energy is left as an important open question.

The author thanks H. Courtois, A. Morpurgo, and S. Russo for many useful suggestions and comments. Special thanks to D. Feinberg and F. Pistolesi for numerous fruitful discussions.

APPENDIX A: DIFFUSION PROBABILITIES IN A NORMAL METAL

1. Diffusion in the electron-electron channel

We first discuss briefly the normal metal diffusion in the ladder approximation. In the Born approximation, the elastic scattering time $\tau_{1;l}$ in the l th Green's function given by

$$g_{1;l}^{A;R}(k;!) = \frac{1}{i\hbar \sum_{i=1;l} \epsilon_i}; \quad (\text{A1})$$

is defined by $k_F^3 \tau_{1;l} v^2 = (4 \epsilon_F) = 1$, with $\tau_{1;l} = \tau_0 [1 + \epsilon_F / \epsilon_l]$, where τ_0 is the elastic scattering time at the Fermi level, v is the amplitude of the microscopic impurity scattering potential, k_F is the Fermi wave-vector, and ϵ_F the Fermi energy.

Using contour integration, and the identity

$$\int_{-\infty}^{\infty} \frac{dk}{(2\pi)^3} f(k) = \frac{1}{8\pi^2} \int_{-1}^{+1} \frac{dk^2}{k^2} \int_{-1}^{+1} du f(k;u) e^{ikR u}; \quad (\text{A2})$$

with $k = k_j$ and $f(k)$ a function of k , we obtain easily

$$\begin{aligned} & \int_{-\infty}^{\infty} \frac{dk}{(2\pi)^3} g_{N}^{1;l}(k) g_{N}^{1;l}(k+q) \\ &= \frac{k_F^3 \tau_{1;l}}{4 \epsilon_F} \frac{1}{1} \frac{D}{4} \frac{1}{q^2 + (l^{(N)})^2}; \end{aligned} \quad (\text{A3})$$

where D is the diffusion constant. The Fourier transform $P^N(q)$ of the diffusion probability $P^N(r)$, given by

$$P^N(q) = t_0^2 \int_{-\infty}^{\infty} \frac{dk}{(2\pi a_0)^3} G_{1;l}^A(k;!) G_{1;l}^R(k+q;!); \quad (\text{A4})$$

where the overline is a disorder averaging and t_0 is the bulk hopping integral (see Eq. (1)), is obtained by summing the ladder series, leading to

$$P^N(q) = \frac{4}{D_0 q^2 + (l^{(N)})^2} : \quad (A 5)$$

In this expression $P^N(q)$ has no dimension. Its Fourier transform $P^N(R)$ is such that $P^N(R)dR$ has no dimension, as expected for a probability.

APPENDIX B : DOUBLE NS INTERFACE

We provide now explanations to the factor $(l^{(N)}=l_e^{(N)})^4$ appearing in Eq. (15) for quasi-two-dimensional normal electrodes. Because of the conservation of the component of the wave-vector parallel to the interface at each tunneling vertex, and because of the form of the diagram, the diagram on Fig. 4 is evaluated at $q_k = 0$, where q_k is the projection of q (see Appendix A) on a plane parallel to the interfaces. By momentum conservation, a finite value of q_k is transformed in $-q_k$ after traversing the entire diagram, so that $q_k = -q_k = 0$. The resulting crossed conductance is thus proportional to $P^N(q_k = 0)^2$, where the square is due to the correlated diffusion in the two normal electrodes, and where the diffusion probability $P^N(q_k)$ is given by Eq. (A 5). This lead to the factor $(l^{(N)}=l_e^{(N)})^4$ since the normal

metals are quasi-two-dimensional so that $q_z = 0$, where q_z is the projection of q on the normal to the interfaces.

APPENDIX C : BALLISTIC N ISIN TRILAYER WITH ATOMIC THICKNESS

We consider in this Appendix a ballistic N ISIN trilayer with atomic thickness^{29,30} in which the three electrodes are two-dimensional, and add a factor $(l^{(N)}=l_e^{(N)})^3$, similar to the factor $(l^{(N)}=l_e^{(N)})^4$ factor discussed previously in the diffusive limit.

The transport formula given by Eq. (9) is Fourier transformed, to obtain

$$G_{a,b}(V_b) = \frac{8}{n} \frac{e^2}{h} t^4 \int \frac{d^2 k}{(2\pi)^2} \text{Tr} \hat{G}_{a;a}^N(k) \hat{G}_3^A(k; eV_b) \hat{G}_{b;b}^N(k) \hat{G}_3^R(k; eV_b) ; \quad (C 1)$$

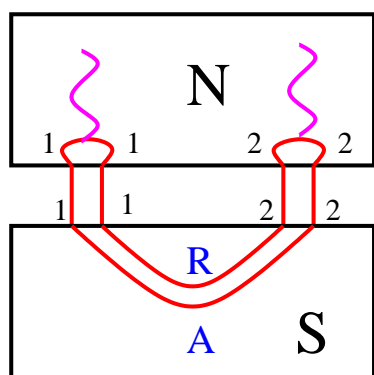
and the Dyson equations for $\hat{G}^{A,R}(k)$ are also Fourier transformed. The normal metal ballistic Green's function is given by $g_{a;a}^{1;1}(k; i) = 1/[i + i\Gamma]$, where Γ is the kinetic energy with respect to the Fermi level, and where the broadening parameter Γ is given by $\Gamma = \sim v_F l^{(N)}$. Eq. (C 1) is then expanded diagrammatically. A diagram similar to the one on Fig. 4 leads to a factor $\Gamma^3 = (\sim v_F l^{(N)})^3$.

-
- * U.P.R. 5001 du CNRS, Laboratoire conventionne avec l'Universite Joseph Fourier
- ¹ M. S. Choi, C. B. Luder, and D. Loss, Phys. Rev. B 62, 13569 (2000); P. Recher, E. V. Sukhorukov, and D. Loss Phys. Rev. B 63, 165314 (2001)
 - ² G. B. Lesovik, T. Martin, and G. Blatter, Eur. Phys. J. B 24, 287 (2001); N. M. Chitchev, G. Blatter, G. B. Lesovik, and T. Martin, Phys. Rev. B 66, 161320 (R) (2002).
 - ³ J. M. Byers and M. E. Flatte, Phys. Rev. Lett. 74, 306 (1995).
 - ⁴ G. Deutscher and D. Feinberg, App. Phys. Lett. 76, 487 (2000);
 - ⁵ P. Samuelson, E. V. Sukhorukov, and M. Buttiker, Phys. Rev. Lett. 91, 157002 (2003).
 - ⁶ E. Prada and F. Sols, Eur. Phys. J. B 40, 379 (2004).
 - ⁷ C. J. Lambert, J. Koltai, and J. Cserti, Towards the Controllable Quantum States (Mesoscopic Superconductivity and Spintronics, 119, Eds H. Takayanagi and J. Nitta, World Scientific (2003).
 - ⁸ D. Beckmann, H. B. Weber, and H. v. Lohneysen, Phys. Rev. Lett. 93, 197003 (2004).
 - ⁹ S. Russo, M. Kroug, T. M. Klapwijk, and A. F. Morpurgo, Phys. Rev. Lett. 95, 027002 (2005).
 - ¹⁰ R. M. Elin and S. Peysson, Phys. Rev. B 68, 174515 (2003); R. M. Elin, Phys. Rev. B 72, 134508 (2005).
 - ¹¹ A. F. Andreev, Sov. Phys. JETP 19, 1228 (1964).

- ¹² C. J. Lambert and R. Raimondi, J. Phys.: Condens. Matter 10, 901 (1998).
- ¹³ F. J. Jedema et al, Phys. Rev. B 60, 16549 (1999).
- ¹⁴ G. Falki, D. Feinberg, and F. W. J. Hekking, Europhysics Letters 54, 255 (2001).
- ¹⁵ The crossed resistance $R_{a,b}(V_b) = @V_a=@I_b(V_b)$, measured experimentally in Ref.⁹, has a sign opposite to the crossed conductance.
- ¹⁶ D. Feinberg, Eur. Phys. J. B 36, 419 (2003).
- ¹⁷ N. M. Chitchev and I. S. Burmistrov, Phys. Rev. B 68, 140501 (2003).
- ¹⁸ R. M. Elin and D. Feinberg, Eur. Phys. J. B 26, 101 (2002).
- ¹⁹ R. M. Elin and D. Feinberg, Phys. Rev. B 70, 174509 (2004).
- ²⁰ A. A. Abrikosov, L. P. Gor'kov, and I. E. Dzyaloshinski, Methods of Quantum Field Theory in Statistical Physics (Dover, New York, 1963).
- ²¹ C. Caroli, R. Combescot, P. Nozières, et D. Saint-James, J. Phys. C 4, 916 (1971); 5, 21 (1972).
- ²² A. Martin-Rodero, F. J. Garcia-Vidal, and A. Levy Yeyati, Phys. Rev. Lett. 72, 554 (1994).
- ²³ A. Levy Yeyati, A. Martin-Rodero, and F. J. Garcia-Vidal, Phys. Rev. B 51, 3743 (1995).
- ²⁴ A. Levy Yeyati, A. Martin-Rodero, and J. C. Cuevas, J. Phys.: Condens. Matter 8, 449 (1996).
- ²⁵ J. C. Cuevas, A. Martin-Rodero and A. Levy Yeyati, Phys. Rev. B 54, 7366 (1996), and references therein.
- ²⁶ R. A. Smith and V. Ambegaokar, Phys. Rev. B 45, 2463

- (1992).
- ²⁷ F.W.J. Hekking and Yu.V. Nazarov, Phys. Rev. Lett. 71, 1625 (1993).
- ²⁸ C. Beenakker, Rev. Mod. Phys. 69, 731 (1997).
- ²⁹ A. Buzdin and M. Daumens, Europhys. Lett. 64, 510 (2003).
- ³⁰ R. Melin and D. Feinberg, Europhys. Lett. 65, 96 (2004)

(a)



(b)

